

The K2 Bright Star Survey

BENJAMIN J. S. POPE,^{1,2,3} TIMOTHY R. WHITE,⁴ CONNY AERTS,^{5,6}
SUZANNE AIGRAIN,⁷ TIMOTHY R. BEDDING,^{8,9} TABETHA BOYAJIAN,¹⁰
ORLAGH L. CREEVEY,¹¹ WILL M. FARR,^{12,13} DAVID W. HOGG,^{1,2,14,15}
DANIEL HUBER,^{16,17,9} AND FRIENDS

¹*Center for Cosmology and Particle Physics, Department of Physics, New York University, 726 Broadway, New York, NY 10003, USA*

²*Center for Data Science, New York University, 60 Fifth Ave, New York, NY 10011, USA*

³*NASA Sagan Fellow*

⁴*Research School of Astronomy and Astrophysics, Mount Stromlo Observatory, The Australian National University, Canberra, ACT 2611, Australia*

⁵*Instituut voor Sterrenkunde, KU Leuven, Celestijnenlaan 200D, B-3001 Leuven, Belgium*

⁶*Department of Astrophysics, IMAPP, Radboud University Nijmegen, P.O. Box 9010, NL-6500 GL Nijmegen, The Netherlands*

⁷*Oxford Astrophysics, Denys Wilkinson Building, University of Oxford, OX1 3RH, Oxford, UK*

⁸*Sydney Institute for Astronomy, School of Physics A28, The University of Sydney, NSW 2006, Australia*

⁹*Stellar Astrophysics Centre, Department of Physics and Astronomy, Aarhus University, DK-8000 Aarhus C, Denmark*

¹⁰*Department of Physics and Astronomy, Louisiana State University, 202 Nicholsom Hall, Baton Rouge, LA 70803, USA*

¹¹*Université Côte d’Azur, Observatoire de la Côte d’Azur, CNRS, Laboratoire Lagrange, Bd de l’Observatoire, CS 34229, 06304 Nice cedex 4, France*

¹²*Center for Computational Astrophysics, Flatiron Institute, 162 Fifth Ave, New York, NY 10010, USA*

¹³*Department of Physics and Astronomy, Stony Brook University, Stony Brook, NY 11794, USA*

¹⁴*Max-Planck-Institut für Astronomie, Königstuhl 17, D-69117 Heidelberg*

¹⁵*Flatiron Institute, 162 Fifth Ave, New York, NY 10010, USA*

¹⁶*Institute for Astronomy, University of Hawai‘i, 2680 Woodlawn Drive, Honolulu, HI 96822, USA*


¹⁷*SETI Institute, 189 Bernardo Avenue, Mountain View, CA 94043, USA*

(Received January 1, 2019; Revised January 7, 2019; Accepted May 16, 2019)

Submitted to ApJ

ABSTRACT

While the *Kepler* Mission was designed to look at tens of thousands of faint stars ($V \gtrsim 12$), brighter stars, which saturate the detector, are important because they can be and have been observed by other instruments at very high signal-to-noise ratio. By considering the unsaturated scattered light ‘halo’ around these stars we can and do retrieve precise light curves of most of the brightest stars in *K2* fields from Campaign 4

onwards. The halo method is highly agnostic about the cause and form of systematics and we show that it nevertheless it is effective at extracting light curves from both normal and saturated stars. The key methodology is to optimize the weights of a linear combination of pixel time series with respect to an objective function. We test a range of such objective functions, finding that generalizations of Total Variation perform well on both saturated and unsaturated *K2* targets. Applying this to the bright stars across the *K2* Campaigns, this reveals stellar variability ubiquitously, including effects of stellar pulsation, rotation, and binarity. Here we describe our pipeline, and present a catalogue of the bright stars studied, with classifications and parametrizations of their variability and remarks on interesting objects. These light curves are publicly available as a High Level Science Product from the Mikulski Archive for Space Telescopes (MAST). 

1. INTRODUCTION

The *Kepler* Space Telescope was launched with a main goal of determining the frequency of Earth-sized planets around Solar-like stars (Borucki et al. 2010), a goal which it has substantially achieved (e.g. Fressin et al. 2013; Petigura et al. 2013; Foreman-Mackey et al. 2014). In order to explore these populations it was necessary to observe hundreds of thousands of stars, with the consequence that the *Kepler* the exposure time and gain were set to optimally observe eleventh or twelfth-magnitude stars, while bright stars are saturated and these saturated stars were intentionally avoided. In the two-wheeled revival as the *K2* mission, the *Kepler* telescope observed a sequence of ecliptic-plane fields containing many more very-saturated stars. While it is difficult to obtain precise light curves of these stars because of their saturation, they are some of the most-valuable targets to follow up with photon-hungry methods such as interferometry or high-resolution spectroscopy, and they typically have long histories of previous observations. Dedicated bright-star space photometry missions such as MOST (Walker et al. 2003) and the BRITE-Constellation (Weiss et al. 2014; Pablo et al. 2016) use very small telescopes (15 and 20 cm apertures respectively), and we would prefer to use much larger telescopes such as *Kepler* (0.95 m) to obtain higher precision lightcurves.

The *Kepler* detector saturates at a magnitude of $K_p \sim 11.3$ in both long- (30 min) and short (1 min)-cadence data, as these both represent sums of 6 s exposures (Gilliland et al. 2010). For objects brighter than this, additional photons create excess electrons which ‘bleed’ into adjacent pixels in both directions along the column containing the bright star. Simple aperture photometry (SAP) – adding all the flux contained in a window around the bleed column – has recovered light curves with precisions close to the photon noise limit of stars as bright as 16 Cyg AB, θ Cyg and RR Lyr (e.g. Kolenberg et al. 2011; White et al. 2013; Guzik et al. 2016). In the nominal *Kepler* mission this was not attempted for all such bright stars, and in *K2*, the several-pixel spacecraft motion significantly increased the size of the required aper-

tures for SAP photometry of very saturated stars, while also making their systematics more difficult to deal with. While the second-version pixel-level-decorrelation (PLD) pipeline EVEREST 2.0 was able to correct systematics in saturated SAP photometry (Luger et al. 2018), this is rendered impossible for the very brightest stars whose bleed columns may run to the edge of the detector. Furthermore, bandwidth constraints meant that pixel data were not downloaded for many bright targets in *K2*.

In order to recover precise photometry of the brightest stars in *K2*, we have therefore developed two main approaches, ‘smear’ and ‘halo’ photometry. Smear photometry (Pope et al. 2016b) uses collateral ‘smear’ calibration data to obtain a 1-D spatial profile with $\sim 1/1000$ of the flux on each CCD. This can be processed to recover light curves of stars which were not necessarily conventionally targeted and downloaded with active pixels, because smear data are recorded for all columns. The main disadvantage of this method is that it confuses all stars in the same column, which means that in crowded fields smear light curves tend to be significantly contaminated.

The more precise method of halo photometry, which is the subject of this paper, uses the broad ‘halo’ of scattered light around a saturated star to recover relative photometry, by constructing a light curve as a linear combination of individual pixel time series and minimizing a Total Variation objective function (TV-min). It has been employed for example on the Pleiades (White et al. 2017) and the brightest-ever star on *Kepler* silicon, Aldebaran (Farr et al. 2018), recovering photometry with a precision nearly that of normally-obtained *K2* observations of unsaturated stars. Unlike smear, this requires downloading data out to a 12–20 pixel radius around each star, and has accordingly only been possible for stars that were specifically targeted with apertures optimized for this method and for a small number of other stars for which this is fortuitously the case. The pixel requirements for this are sufficiently low that, with the help of the *K2* Guest Observer office, such apertures were obtained for most of the bright targets from Campaign 4 onwards.

In this Paper we describe numerical experiments testing the TV-min method and extending it to generalizations with different exponents and timescales. We show that the method as previously employed applying standard TV-min is suboptimal, and gain a modest improvement from taking finite differences close to the timescale of *K2* thruster firings. We go on to present complete catalog of long-cadence *K2* halo light curves, which we have made publicly available. We have employed halo photometry on all stars targeted with appropriate apertures, and have done a preliminary characterization of interesting astrophysical variability. We also document the main changes in the halo data reduction pipeline, **halophot**, with respect to previous releases. These include oscillating red giants, pulsating and quiet main sequence stars, and eclipsing binaries, many of which are among the brightest objects of their type to have been observed with space photometry. We hope that this diverse catalog of light curves will be useful for an equally-diverse range of astrophysical investigations.

2. HALO PHOTOMETRY METHOD

This method was first described by [White et al. \(2017\)](#) and applied to the Pleiades’ Seven Sisters, and was applied to Aldebaran with further developments by [Farr et al. \(2018\)](#). Because SAP is not possible, we consider instead the unsaturated pixels p_j at the wings of the broad and structured PSF. We construct a light curve as a linear combination of these time series with weights w_j , so that flux at cadence i is

$$f_i \equiv \sum_j w_j p_{ij}. \quad (1)$$

In our updated pipeline presented here, the weights are chosen to minimize an objective function

$$Q_{k,l} \equiv \sum_i |f_i - f_{i-\delta}|^k, \quad (2)$$

subject to the constraints

$$\forall_j w_j > 0 \quad (3)$$

$$\sum_{i=1}^N f_i = N. \quad (4)$$

This is a classic convex optimization program with constraints, which we solve with the `scipy` ([Jones et al. 2001](#)) L-BFGS-B nonlinear optimization code ([Zhu et al. 1999](#)). $Q_{k,l}$ has analytic derivatives with respect to w_j (calculated with `autograd`; [Maclaurin et al. 2015](#)), and it is therefore extremely fast to optimize and converges well on a global solution. In practice, for computational reasons we optimize over parameters \tilde{w}_j such that $w_j = \text{softmax}(\tilde{w}_j)$, as this satisfies the constraint that $\forall_j w_j > 0$, and while this also constrains their sum to be unity, we renormalize f to satisfy its normalization constraint before calculating the objective function and this additional constraint is removed again.

The objective function $Q_{k,l}$ is the L_k norm on a ‘lagged’ finite difference with a lag parameter δ . For $k = 1$ and $\delta = 1$, $Q_{1,1}$ is the standard Total Variation objective (TV) used in previous halo papers (e.g. [White et al. 2017](#); [Farr et al. 2018](#)), and can be seen as the L1 norm on the derivative of f or as a discrete approximation to its arc length. The L2 Variation (L2V) with $k = 2$ is sometimes referred to in image processing literature as the ‘smoothness’ regularizer, as it seeks to penalize large gradients without necessarily making them sparse. The lag parameter δ allows for flexibility in modelling systematics occurring at different timescales from cadence-to-cadence, and we investigate its effects below. The order parameter k allows for flexibility in how sensitive we are to normally-distributed versus long-tailed noise. For convenience in the rest of this paper, we will refer to the $k = 1$ case as TV, the $k = 2$ case as L2V, and the $k = 3$ case as L3V.

Unlike other methods for calibrating *Kepler* systematics, other than the value of δ , no knowledge of the spacecraft motion or the behaviour of an ensemble of other stars is used to inform our algorithm. The method is a self-calibration that is independent of the details of the systematics it is calibrating, operating on the assumption that a single signal is present across many individual time series which otherwise are contaminated by noise. It is therefore likely that significant improvements can be made to the method by including cotrending basis vectors with mean zero and whose weights are allowed to be negative, which would represent systematics which are common to all pixels in the halo aperture and therefore masquerade as signal. Any linear combination of convex objective functions is itself convex, and future extensions to the method could enforce combinations of different lags and orders to better represent systematics occurring on different timescales (e.g. thruster firings, red noise) and with different levels of smoothness.

In addition to expanding the range of possible objective functions, we have also added a feature ‘deathstar’ to deal with contamination. We apply the watershed-based image segmentation algorithm from K2P2 (Lund et al. 2015) to the input target pixel file datacube to identify possible background sources and cut them out. [More here from Tim.](#) Other than this, we have adopted less-aggressive quality flagging, having found that many cadences were being classified as bad quality for spurious ‘cosmic ray’ events, which were actually caused by a combination of saturation and spacecraft motion. We now iteratively sigma-clip outliers and retain cadences with the `lightkurve` default quality mask.

While the halo procedure produces in most cases a fairly clean light curve, there are nevertheless residual systematic errors related to spacecraft motion. In order to correct these, we employ the K2SC code (Aigrain et al. 2015, 2016), which simultaneously models a light curve as a 3D Gaussian Process (GP) in time and predicted position (the K2 standard data product POS_CORR) in pixels (x, y) . The model prediction in time for fixed position is then a nonparametric model of the stellar variability, and the prediction for the x, y component evaluated for fixed time represents the pointing systematics. We subtract the systematics model from the input fluxes to obtain a final corrected flux, which is the time series we use and recommend for science. The target pixel files for C91, C92, and C101 include no position information, and there are no halo apertures for C112. As a result K2SC-corrected data are not available for these targets.

2.1. Choosing the Objective Function

In order to choose the values for k and δ in our objective function, we have selected the quiet star 36 Ophiuchi, the lowest-mass main sequence star in the sample of stars with halo apertures, and one with very little high frequency variability detected or predicted, which was also observed at short cadence. We choose the 6.5 hour Combined Differential Photometric Precision (CDPP, Christiansen et al. 2012) as

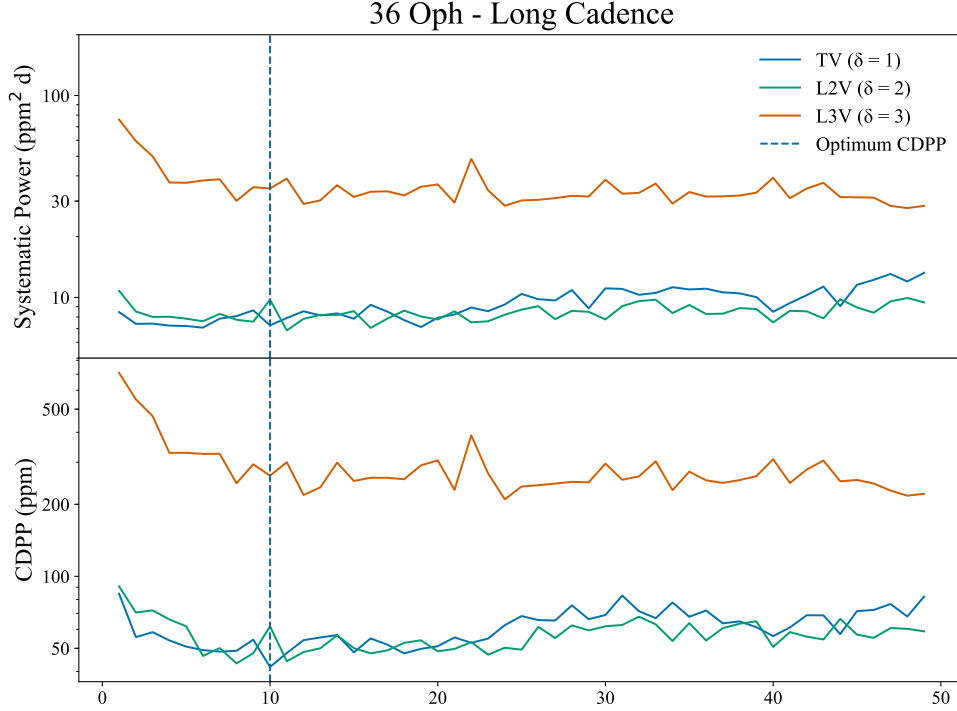


Figure 1. Behaviour of long cadence 6.5 hour CDPP (bottom) and $4c/d$ systematics power (top) for the quiet dwarf 36 Ophiuchi as a function of lag parameter δ . CDPP shows a minimum for L1 norm and $\delta = 10$, i.e. for objective function $Q_{1,10}$, which is marked with a blue dashed vertical line. This does not correspond to an optimum in systematic power, which is slightly lower for smaller δ . Nevertheless, we have chosen $\delta = 10$ for the light curves in this catalog because of its improvement in overall CDPP as a measure of planet detection efficiency and overall light curve quality.

implemented in `lightkurve` (Vinícius et al. 2018) as a proxy for the ‘noise’ in a lightcurve, with lower being better. We calculate halo lightcurves and their CDPPs for $k \in \{1, 2, 3\}$, and $\delta \in [1, 50]$ for long cadence and for various values of $\delta \in [1, 2500]$ for short cadence data. The results are displayed in Figures 1 and 2. We find that for long cadence data, $k = 1$ (TV) and a lag $\delta = 10$ provide the best CDPP. This is unsurprising: that this is one cadence shorter than the 12 cadence thruster firing period. In this context we can understand the optimum as suppressing systematics on the same timescale as they occur. On the other hand, for short cadence data, performance at short lags is very poor but the method performs similarly for $k \in \{1, 2\}$ with slow improvement with larger δ , and performs very poorly for $k = 3$ at all lags.

We accordingly use a lag $\delta = 10$ for all long cadence light curves, and a lag $\delta = 300$ for short cadence for consistency in timescale with the long cadence processing.

2.2. Benchmarking

As the halo method is the only available means of obtaining light curves of stars as bright as in our sample, and they are ubiquitously found to be variable, it is difficult based on this sample alone to determine the accuracy and precision of the light curves obtained. While Kallinger & Weiss (2018) have found agreement between the White

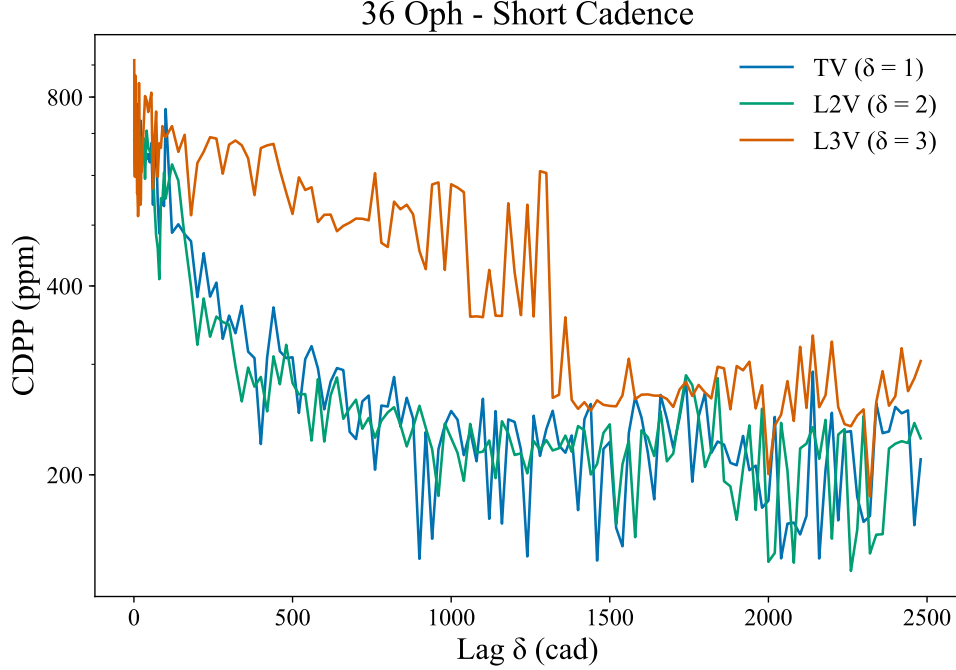


Figure 2. Behaviour of short cadence 6.5 hour CDPP for the quiet dwarf 36 Ophiuchi as a function of lag parameter δ . CDPP continuously improves for higher lags and shows no strong differences between L1 and L2 norms, while L3 performs poorly.

et al. (2017) halo observations of Atlas and their BRITe-Constellation observations, the BRITe observations have a lower precision and cannot be obtained for most of the stars in our sample.

We want to compare the photometric precision obtained to that from SAP and normal calibration pipelines, and ascertain whether we systematically distort the scale of variation or the power spectrum of variability. In order to do this, we take the sample of stars with $11.5 < Kp < 12.5$ from *K2* Campaign 6, for which *k2SC* light curves are available, choosing 2466 stars that are as bright as possible without saturation. The planets in this campaign are well characterized (e.g. Pope et al. 2016a), and eight singly-transiting systems are known in this magnitude range. We take the entire target pixel file without using any aperture restriction, and run TV-min with $\delta = 10$ for each of these planets and compare these to light curves from the PDC pipeline. In both cases, we correct residual systematics with *k2SC*, prewhiten with the GP time trend model, clip 3σ upwards outliers, and normalize the final fluxes to unity. These are then folded on the known transit period and zero epoch as tabulated in the NASA Exoplanet Archive (Akeson et al. 2013), and the folded lightcurves are binned in 3-cadence bins to reduce white noise in the comparison. The results are displayed in Figure 2.2.

We now seek to establish the global noise properties of the whole unsaturated sample, and compare these to PDC. We process all 2466 stars with TV-min and $\delta = 10$, using all pixels in the TPF unmasked. Because these stars are so bright and the TPFs

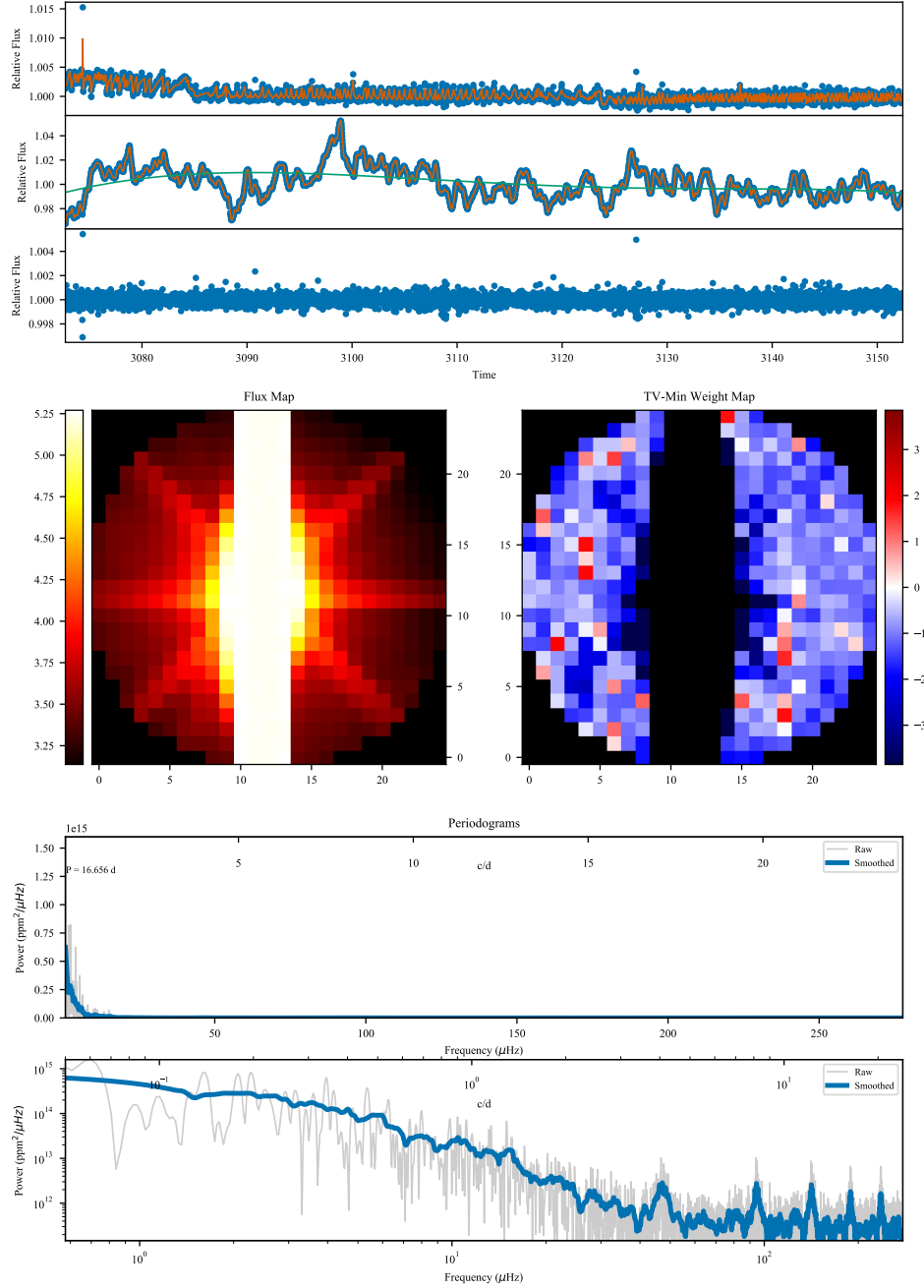
ρ Leo (EPIC 200182931) Detrended

Figure 3. Summary plots for K2SC-corrected final halo light curve for ρ Leonis. The top three panels illustrate K2SC systematics correction: at the top, flux minus the GP time trend (blue dots) with GP x, y trend superimposed (orange line); in the middle, flux minus GP x, y components with GP time trend superimposed, and in green, a fifteenth-order polynomial trend; at the bottom the ‘whitened’ light curve with flux minus both GP components. Middle two panels: log-flux map (left) and halo log-weight map (right). Bottom two panels: periodograms in linear (top) and log (bottom) units of the residuals of the corrected light curve minus the long term polynomial trend. Plots of this form are available in supplementary online material for all long-cadence stars, together with similar plots for all short-cadence stars but without K2SC. The period at maximum power (16 d) is marked on all plots, though for ρ Leonis all variability is consistent with red noise (Bowman et al. 2019).

Campaign 6 Planets

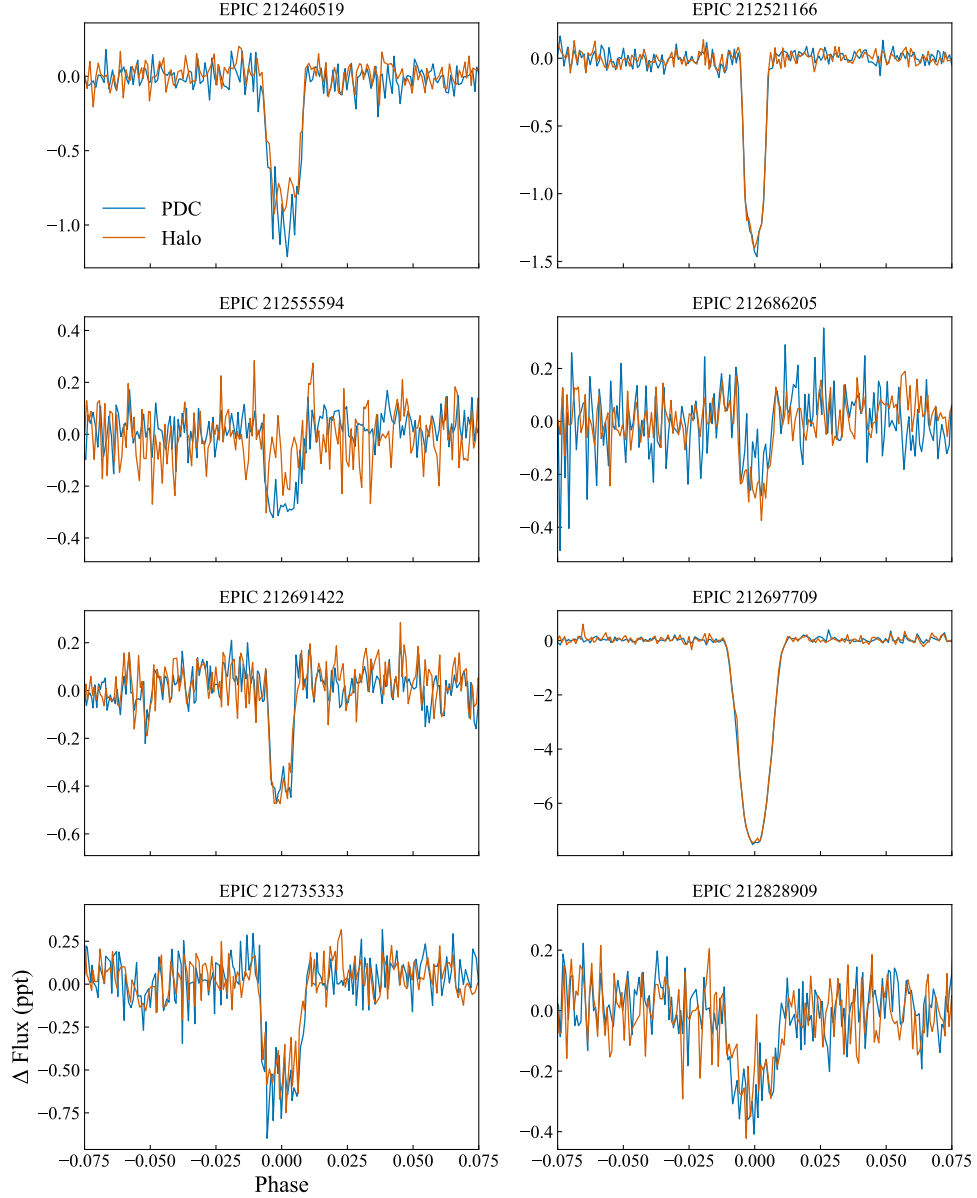


Figure 4. The eight transiting single-planet systems in *K2* Campaign 6 in the magnitude range $11.5 < Kp < 12.5$, with PDC light curves (blue) and TV-min light curves (orange) overlaid. These have been identically *k2sc*-corrected, whitened, outlier-clipped, folded and binned as described in Section 2.2. The depths and shapes of the transits agree closely except for EPIC 212460519, for which the TV-min transit is slightly shallower, and EPIC 212555594, for which TV-min is significantly shallower.

so small, in the great majority of cases we do not expect significant contamination, and this is a way of testing how well the weights assigned by TV-min match the flux distribution over pixels.

3. SAMPLE

The full sample of stars for which halo apertures were obtained is listed in Table 1. While some very bright stars were observed with conventional apertures as part of these programs, simple aperture photometry is satisfactory on these targets and we exclude them from the present discussion and data release, which is oriented strictly towards targets only observable with halo photometry. We make an exception for Spica, which was observed in Campaign 6 without a halo aperture but in Campaign 17 with a halo aperture. In Campaign 6 it was assigned a normal aperture by mistake and simple aperture photometry performed extremely poorly, so we have processed it with the halo pipeline. The stars in Campaign 18 were also on-silicon in Campaign 5, but were not assigned apertures suitable for halo photometry in C5. A possible further extension of the present work would be to recover C5 light curves for these objects using either or both of smear or modified halo photometry.

Seven stars in Campaign 13 and one in Campaign 16 were not only assigned long-cadence halo apertures, but also downloaded at short cadence. For these targets we have provided both long and short cadence reductions. Following the analysis in Section 2 showing the insensitivity of short cadence CDPP to lags longer than ~ 100 cad and on choice of objective function, for consistency with long cadence we have adopted a 300 cadence lag (i.e. $30\times$ the long cadence lag of 10) and the L1 TV objective function. With their long timeseries the short cadence stars are computationally intractable for the Gaussian Process model in $\kappa 2\text{SC}$ and we present otherwise uncalibrated halo lightcurves.

Analyses for several of the objects here have been previously published, but we here provide the first public data releases for the Pleiades’ Seven Sisters (White et al. 2017), Aldebaran (Farr et al. 2018), ι Lib (Buysschaert et al. 2018), and ϵ Tau (Arentoft et al. 2019), as well as ρ Leo which was studied with halo pixels but without our objective functions (Aerts et al. 2018).

4. DISCUSSION

4.1. *Oscillating Red Giants*

31 of the evolved stars in our sample have detectable stochastically-excited solar-like acoustic oscillations. In the asymptotic limit, these consist of a comb of modes separated by the large frequency separation $\Delta\nu$, approximately the sound-crossing-time of the star, with a Gaussian envelope centred on the frequency of maximum power ν_{max} , which scales with the acoustic cutoff frequency at the star’s surface. These can be used to constrain stellar fundamental parameters, and detailed studies of the deviations from this asymptotic limit for acoustic p -modes, for example due to their interaction with gravity-wave g -modes, can be used to accurately determine the stellar evolutionary state, for example to distinguish hydrogen shell burning red giant branch from helium core burning red clump stars.

Using the Sydney pipeline (Huber et al. 2009) with modifications to the extraction of $\Delta\nu$ detailed in (Yu et al. 2018), we extract the global asteroseismic parameters ν_{max}

and $\Delta\nu$ for all 31 giants for which oscillations are detected. These parameters are listed in Table 2. High precision spectroscopy of these stars would permit detailed stellar modelling and the extraction of precise elemental abundances, which would make these stars valuable as benchmarks for large spectroscopic surveys or testing detailed stellar models. This sample would be a valuable addition to the 36 Gaia FGK benchmark stars (Jofré et al. 2014; Heiter et al. 2015; Jofré et al. 2018) and the 33 *Kepler* Smear Campaign spectroscopic benchmark red giants (Pope et al., 2019, under review).

4.2. Classical Variables

Variability catalog?

4.3. Chemically-Peculiar Stars

The chemically-peculiar A0V star 98 Tau is of special interest for studies of surface inhomogeneity. We detect variability with a fundamental period of 1.74 d with twice as much power at the first harmonic ($P = 0.87$ d), which is consistent with α^2 CVn spot modulation from a rapidly-rotating star with a period of 1.74 d. This star also experiences a transit of depth 0.03, which for a $1.87 R_{\odot}$ typical A0V star imply an $0.3 R_{\odot}$ companion, almost certainly of stellar mass. With rotational modulation and an eclipse to break degeneracies, models such as *starry* (Luger et al. 2019) can infer surface brightness maps and reveal the spatial distribution of the star’s chemical peculiarity.

5. CONCLUSIONS

Some of the objects presented here are the subject of more detailed work in preparation, namely Spica (Buzasi et al., in prep.), the Hyades giants (White et al., in prep.), and main-sequence stars (Grekle-McKeon et al., in prep.).

The sample of K2 bright stars presented here only includes those with halo apertures, but while some others are available conventionally, many were not assigned target pixels and were not downloaded at all. Smear photometry has been used to recover the brightest otherwise-unobserved stars in nominal *Kepler* (Pope et al., under review), and this can also be done in K2, although in the latter case the sample is much smaller due to competition with halo apertures and the systematics correction is more challenging. A natural extension of both pieces of work would be to produce smear light curves of all bright stars without halo apertures in K2, which would finally make the *Kepler* extended mission magnitude-complete at the bright end.

The halo method naturally extends to other contexts where simple aperture photometry is not possible, such as for saturated stars observed by the Transiting Exoplanet Survey Satellite (TESS; Ricker et al. 2015). Although the saturation limit is brighter ($T_{mag} \sim 6$) and this problem accordingly affects fewer stars and less badly, there are situations such as for α Centauri or β Hydri where the bleed column reaches the edge of the chip and a SAP light curve is irrecoverable. We expect that TV-min halo

photometry will therefore be valuable in ensuring that TESS can observe even the very brightest stars.

ACKNOWLEDGEMENTS

This work was performed in part under contract with the Jet Propulsion Laboratory (JPL) funded by NASA through the Sagan Fellowship Program executed by the NASA Exoplanet Science Institute. TRW acknowledges the support of the Australian Research Council (grant DP150100250) and the Villum Foundation (research grant 10118). The halo apertures were kindly provided by the K2 team as part of the Guest Observer programs GO6081-7081, GO8025, GO9923, GO10025, GO11047-13047, GO14003-16003, and GO17051-19051, and as a Director’s Discretionary Time program in Campaign 4 as GO4901. We are grateful for the associated funding provided by the K2 GO office which has been essential in bringing this project to fruition.

This project was developed in part at the Building Early Science with TESS meeting, which took place in March 2019 at the University of Chicago.

BJSP acknowledges being on the traditional territory of the Lenape Nations and recognizes that Manhattan continues to be the home to many Algonkian peoples. We give blessings and thanks to the Lenape people and Lenape Nations in recognition that we are carrying out this work on their indigenous homelands. We would like to acknowledge the Gadigal Clan of the Eora Nation as the traditional owners of the land on which the University of Sydney is built and on which some of this work was carried out, and pay their respects to their knowledge, and to their elders past, present, and future.

This research made use of NASA’s Astrophysics Data System; the SIMBAD database, operated at CDS, Strasbourg, France. Some of the data presented in this paper were obtained from the Mikulski Archive for Space Telescopes (MAST). STScI is operated by the Association of Universities for Research in Astronomy, Inc., under NASA contract NAS5-26555. Support for MAST for non-HST data is provided by the NASA Office of Space Science via grant NNX13AC07G and by other grants and contracts. We acknowledge the support of the Group of Eight universities and the German Academic Exchange Service through the Go8 Australia-Germany Joint Research Co-operation Scheme.

Software: IPython (Pérez & Granger 2007); SciPy (Jones et al. 2001); and Astropy, a community-developed core Python package for Astronomy (Astropy Collaboration et al. 2013).

REFERENCES

- | | |
|--|---|
| <p>Aerts, C., Bowman, D. M., Símón-Díaz, S., et al. 2018, MNRAS, 476, 1234, doi: 10.1093/mnras/sty308</p> | <p>Aigrain, S., Hodgkin, S. T., Irwin, M. J., Lewis, J. R., & Roberts, S. J. 2015, MNRAS, 447, 2880, doi: 10.1093/mnras/stu2638</p> |
|--|---|

- Aigrain, S., Parviainen, H., & Pope, B. J. S. 2016, *MNRAS*, 459, 2408, doi: [10.1093/mnras/stw706](https://doi.org/10.1093/mnras/stw706)
- Akeson, R. L., Chen, X., Ciardi, D., et al. 2013, *PASP*, 125, 989, doi: [10.1086/672273](https://doi.org/10.1086/672273)
- Arentoft, T., Grundahl, F., White, T. R., et al. 2019, *A&A*, 622, A190, doi: [10.1051/0004-6361/201834690](https://doi.org/10.1051/0004-6361/201834690)
- Astropy Collaboration, Robitaille, T. P., Tollerud, E. J., et al. 2013, *A&A*, 558, A33, doi: [10.1051/0004-6361/201322068](https://doi.org/10.1051/0004-6361/201322068)
- Borucki, W. J., Koch, D., Basri, G., et al. 2010, *Science*, 327, 977, doi: [10.1126/science.1185402](https://doi.org/10.1126/science.1185402)
- Bowman, D. M., Burssens, S., Pedersen, M. G., et al. 2019, arXiv e-prints, arXiv:1905.02120, <https://arxiv.org/abs/1905.02120>
- Buysschaert, B., Neiner, C., Aerts, C., White, T. R., & Pope, B. J. S. 2018, in *SF2A-2018: Proceedings of the Annual meeting of the French Society of Astronomy and Astrophysics*, 369–372
- Christiansen, J. L., Jenkins, J. M., Caldwell, D. A., et al. 2012, *Publications of the Astronomical Society of the Pacific*, 124, 1279, doi: [10.1086/668847](https://doi.org/10.1086/668847)
- Farr, W. M., Pope, B. J. S., Davies, G. R., et al. 2018, *ApJ*, 865, L20, doi: [10.3847/2041-8213/aadfde](https://doi.org/10.3847/2041-8213/aadfde)
- Foreman-Mackey, D., Hogg, D. W., & Morton, T. D. 2014, *ApJ*, 795, 64, doi: [10.1088/0004-637X/795/1/64](https://doi.org/10.1088/0004-637X/795/1/64)
- Fressin, F., Torres, G., Charbonneau, D., et al. 2013, *ApJ*, 766, 81, doi: [10.1088/0004-637X/766/2/81](https://doi.org/10.1088/0004-637X/766/2/81)
- Gilliland, R. L., Jenkins, J. M., Borucki, W. J., et al. 2010, *ApJL*, 713, L160, doi: [10.1088/2041-8205/713/2/L160](https://doi.org/10.1088/2041-8205/713/2/L160)
- Guzik, J. A., Houdek, G., Chaplin, W. J., et al. 2016, *ApJ*, 831, 17, doi: [10.3847/0004-637X/831/1/17](https://doi.org/10.3847/0004-637X/831/1/17)
- Heiter, U., Jofré, P., Gustafsson, B., et al. 2015, *A&A*, 582, A49, doi: [10.1051/0004-6361/201526319](https://doi.org/10.1051/0004-6361/201526319)
- Huber, D., Stello, D., Bedding, T. R., et al. 2009, *Communications in Asteroseismology*, 160, 74, <https://arxiv.org/abs/0910.2764>
- Jofré, P., Heiter, U., Tucci Maia, M., et al. 2018, *Research Notes of the American Astronomical Society*, 2, 152, doi: [10.3847/2515-5172/aadc61](https://doi.org/10.3847/2515-5172/aadc61)
- Jofré, P., Heiter, U., Soubiran, C., et al. 2014, *A&A*, 564, A133, doi: [10.1051/0004-6361/201322440](https://doi.org/10.1051/0004-6361/201322440)
- Jones, E., Oliphant, T., Peterson, P., & Others. 2001, *SciPy: Open source scientific tools for Python*, <http://www.scipy.org/>
- Kallinger, T., & Weiss, W. W. 2018, in *3rd BRITE Science Conference*, Vol. 8, 170–174
- Kolenberg, K., Bryson, S., Szabó, R., et al. 2011, *MNRAS*, 411, 878, doi: [10.1111/j.1365-2966.2010.17728.x](https://doi.org/10.1111/j.1365-2966.2010.17728.x)
- Luger, R., Agol, E., Foreman-Mackey, D., et al. 2019, *AJ*, 157, 64, doi: [10.3847/1538-3881/aae8e5](https://doi.org/10.3847/1538-3881/aae8e5)
- Luger, R., Kruse, E., Foreman-Mackey, D., Agol, E., & Saunders, N. 2018, *AJ*, 156, 99, doi: [10.3847/1538-3881/aad230](https://doi.org/10.3847/1538-3881/aad230)
- Lund, M. N., Handberg, R., Davies, G. R., Chaplin, W. J., & Jones, C. D. 2015, *ApJ*, 806, 30, doi: [10.1088/0004-637X/806/1/30](https://doi.org/10.1088/0004-637X/806/1/30)
- Maclaurin, D., Duvenaud, D., & Adams, R. P. 2015, in *ICML 2015 AutoML Workshop*
- Pablo, H., Whittaker, G. N., Popowicz, A., et al. 2016, *PASP*, 128, 125001, doi: [10.1088/1538-3873/128/970/125001](https://doi.org/10.1088/1538-3873/128/970/125001)
- Pérez, F., & Granger, B. E. 2007, *Computing in Science and Engineering*, 9, 21, doi: [10.1109/MCSE.2007.53](https://doi.org/10.1109/MCSE.2007.53)
- Petigura, E. A., Howard, A. W., & Marcy, G. W. 2013, *Proceedings of the National Academy of Science*, 110, 19273, doi: [10.1073/pnas.1319909110](https://doi.org/10.1073/pnas.1319909110)
- Pope, B. J. S., Parviainen, H., & Aigrain, S. 2016a, *MNRAS*, 461, 3399, doi: [10.1093/mnras/stw1373](https://doi.org/10.1093/mnras/stw1373)
- Pope, B. J. S., White, T. R., Huber, D., et al. 2016b, *MNRAS*, 455, L36, doi: [10.1093/mnras/slv143](https://doi.org/10.1093/mnras/slv143)

- Ricker, G. R., Winn, J. N., Vanderspek, R., et al. 2015, *Journal of Astronomical Telescopes, Instruments, and Systems*, 1, 014003, doi: [10.1117/1.JATIS.1.1.014003](https://doi.org/10.1117/1.JATIS.1.1.014003)
- Vinícius, Z., Barentsen, G., Hedges, C., & Gully-Santiago, M. 2018, *KeplerGO/lightkurve: 1.0.0.dev1: First development release of lightkurve*, doi: [10.5281/zenodo.1181929](https://doi.org/10.5281/zenodo.1181929). <https://doi.org/10.5281/zenodo.1181929>
- Walker, G., Matthews, J., Kuschnig, R., et al. 2003, *PASP*, 115, 1023, doi: [10.1086/377358](https://doi.org/10.1086/377358)
- Weiss, W. W., Rucinski, S. M., Moffat, A. F. J., et al. 2014, *PASP*, 126, 573, doi: [10.1086/677236](https://doi.org/10.1086/677236)
- White, T. R., Huber, D., Maestro, V., et al. 2013, *MNRAS*, 433, 1262, doi: [10.1093/mnras/stt802](https://doi.org/10.1093/mnras/stt802)
- White, T. R., Pope, B. J. S., Antoci, V., et al. 2017, *MNRAS*, 471, 2882, doi: [10.1093/mnras/stx1050](https://doi.org/10.1093/mnras/stx1050)
- Yu, J., Huber, D., Bedding, T. R., et al. 2018, *ApJS*, 236, 42, doi: [10.3847/1538-4365/aaaf74](https://doi.org/10.3847/1538-4365/aaaf74)
- Zhu, C., H. Byrd, R., & Lu, P. 1999

APPENDIX

Table 1. All stars observed with halo photometry in K2.

| Name | EPIC | Spectral Type | V (mag) | Campaign | Comments |
|----------------|-----------|-----------------------|------------|----------|-------------|
| Alcyone | 200007767 | B7III | 2.986 | 4 | a |
| Atlas | 200007768 | | 3.763 | 4 | a |
| Electra | 200007769 | B6IIIe | 3.851 | 4 | a |
| Merope | 200007770 | B6IVe | 4.305 | 4 | a |
| Maia | 200007771 | B8III | 4.305 | 4 | a |
| Taygeta | 200007772 | B6IV | 4.448 | 4 | a |
| Pleione | 200007773 | B8Vne | 5.192 | 4 | a |
| γ Tau | 200007765 | G9.5IIIabCN0.5 | 3.474 | 4 | |
| δ 1 Tau | 200007766 | G9.5IIICN0.5 | 3.585 | 4 | |
| Spica | 212573842 | B1V | 0.97 | 6, 17 | Normal Mask |
| 69 Vir | 212356048 | K0III-IIIbCN1.5CH0.5 | 4.75 | 6 | |
| Ascella | 200062593 | A2.5Va | 2.585 | 7 | |
| Albaldah | 200062592 | F2II-III | 2.88 | 7 | |
| τ Sgr | 200062591 | K1.5IIIb | 3.31 | 7 | |
| ξ 2 Sgr | 200062590 | G8/K0II/III | 3.51 | 7 | |
| o Sgr | 200062589 | G9IIIb | 3.77 | 7 | |
| 52 Sgr | 200062585 | B8/9V | 4.598 | 7 | |
| Ainalrami | 200062588 | K1II | 4.845 | 7 | |
| ψ Sgr | 200062584 | K0/1III+A/F | 4.85 | 7 | |
| 43 Sgr | 200062587 | G8II-III | 4.878 | 7 | |
| ν 2 Sgr | 200062586 | K3-II-III:CN1Ba1 | 4.98 | 7 | |
| ϵ Psc | 200068392 | G9IIIbFe-2 | 4.28 | 8 | |
| Revati | 200068393 | A7IV | 5.187 | 8 | |
| 80 Psc | 200068394 | F2V | 5.5 | 8 | |
| 42 Cet | 200068399 | G8IV+A(8) | 5.87 | 8 | |
| 33 Cet | 200068395 | K4/5III | 5.942 | 8 | |
| 60 Psc | 200068396 | G8III | 5.961 | 8 | |
| 73 Psc | 200068397 | K5III | 6.007 | 8 | |
| WW Psc | 200068398 | M2.5III | 6.14 | 8 | |
| HR 243 | 200068400 | G8/K0II/III | 6.368 | 8 | |
| HR 161 | 200068401 | K3III | 6.407 | 8 | |
| HR 6766 | 200069361 | G7:IIIbCN-1CH-3.5HK+1 | 4.56 | 9 | |
| HR 6842 | 200069360 | K3II | 4.627 | 9 | |
| 4 Sgr | 200069357 | A0 | 4.724 | 9 | |

Table 1 continued on next page

Table 1 (*continued*)

| Name | EPIC | Spectral Type | V (mag) | Campaign | Comments |
|--------------|-----------|------------------|------------|----------|----------|
| 11 Sgr | 200069358 | K0III | 4.98 | 9 | |
| 7 Sgr | 200069362 | F2II-III | 5.34 | 9 | |
| 15 Sgr | 200069359 | O9.7Iab | 5.37 | 9 | |
| HR 6838 | 200069363 | K2III | 5.75 | 9 | |
| Y Sgr | 200069364 | F8II | 5.75 | 9 | Cepheid |
| HR 6716 | 200069365 | B0Iab/b | 5.77 | 9 | |
| HR 6681 | 200069366 | A0V | 5.929 | 9 | |
| 9 Sgr | 200069368 | O4V((f))z | 5.97 | 9 | |
| 16 Sgr | 200069367 | O9.5III | 6.02 | 9 | |
| HR 6825 | 200069369 | ApSi | 6.15 | 9 | |
| 63 Oph | 200069370 | O8II((f)) | 6.2 | 9 | |
| HR 6679 | 200069373 | A1V | 6.469 | 9 | |
| HD 165784 | 200069371 | A2Iab | 6.58 | 9 | |
| HD 161083 | 200069374 | F0V | 6.58 | 9 | |
| 5 Sgr | 200069372 | K0III | 6.64 | 9 | |
| HD 167576 | 200069378 | K1III | 6.66 | 9 | |
| HR 6773 | 200069380 | B3/5IV | 6.71 | 9 | |
| HD 163296 | 200071159 | A1Vep | 6.85 | 9 | |
| HD 165052 | 200069379 | O5.5:Vz+O8:V | 6.87 | 9 | |
| 17 Sgr | 200069375 | G8/K0III | 6.886 | 9 | |
| HD 169966 | 200069376 | G8/K0III | 6.97 | 9 | |
| HD 162030 | 200069377 | K1III | 7.02 | 9 | |
| Porrima | 200084004 | F1V+F0mF2V | 2.74 | 10 | |
| Zaniah | 200084005 | A2IV | 3.9 | 10 | |
| 21 Vir | 200084006 | B9V | 5.48 | 10 | |
| FW Vir | 200084007 | M3+IIICa0.5 | 5.71 | 10 | |
| HR 4837 | 200084008 | G8III | 5.918 | 10 | |
| HR 4591 | 200084009 | K1III | 6.316 | 10 | |
| HR 4613 | 200084010 | G8/K0III | 6.364 | 10 | |
| HD 107794 | 200084011 | K0III | 6.46 | 10 | |
| θ Oph | 200128906 | OB | 3.26 | 11 | |
| 44 Oph | 200128907 | kA5hA9mF1III | 4.153 | 11 | |
| 45 Oph | 200128908 | F5III-IV | 4.269 | 11 | |
| 51 Oph | 200128909 | A0V | 4.81 | 11 | |
| 36 Oph | 200129035 | K2V+K1V | 5.03 | 11 | |
| o Oph | 200128910 | | 5.2 | 11 | |
| 26 Oph | 200129034 | F3V | 5.731 | 11 | |
| HR 6472 | 200128911 | K0III | 5.83 | 11 | |

Table 1 continued on next page

Table 1 (*continued*)

| Name | EPIC | Spectral Type | V (mag) | Campaign | Comments |
|----------------|-----------|------------------|------------|----------|--------------|
| HR 6366 | 200128913 | Fm dD | 5.911 | 11 | |
| HR 6365 | 200128912 | K0III | 5.977 | 11 | |
| 191 Oph | 200128914 | K0III | 6.171 | 11 | |
| κ Psc | 200164167 | A2VpSrCrSi | 4.94 | 12 | |
| 83 Aqr | 200164168 | F0V | 5.47 | 12 | |
| 24 Psc | 200164169 | K0II/III | 5.94 | 12 | |
| HR 8759 | 200164170 | G5II/III | 5.933 | 12 | |
| 14 Psc | 200164171 | A2II | 5.87 | 12 | |
| HR 8921 | 200164172 | K4/5III | 6.191 | 12 | |
| 81 Aqr | 200164173 | K4III | 6.215 | 12 | |
| HR 8897 | 200164174 | K4III | 6.34 | 12 | |
| Aldebaran | 200173843 | K5+III | 0.86 | 13 | ^c |
| θ 2 Tau | 200173845 | A7III | 3.41 | 13 | SC |
| ϵ Tau | 200173844 | G9.5IIICN0.5 | 3.53 | 13 | ^d |
| θ 1 Tau | 200173846 | G9IIIFe-0.5 | 3.84 | 13 | |
| κ 1 Tau | 200173847 | A7IV-V | 4.201 | 13 | SC |
| δ 3 Tau | 200173849 | A2IV-Vs | 4.25 | 13 | C4 |
| τ Tau | 200173850 | B3V | 4.258 | 13 | |
| ν Tau | 200173848 | A8Vn | 4.282 | 13 | SC |
| ρ Tau | 200173851 | A8V | 4.65 | 13 | SC |
| 11 Ori | 200173853 | A1VpSiCr | 4.661 | 13 | |
| HR 1427 | 200173855 | A6IV | 4.764 | 13 | SC |
| 15 Ori | 200173854 | F2IV | 4.82 | 13 | |
| 75 Tau | 200173852 | K1IIIb | 4.969 | 13 | |
| 97 Tau | 200173857 | A7IV-V | 5.085 | 13 | SC |
| HR 1684 | 200173856 | K5III | 5.163 | 13 | |
| κ 2 Tau | 200173859 | F0Vn | 5.264 | 13 | SC |
| 56 Tau | 200173861 | A0VpSi | 5.346 | 13 | |
| 81 Tau | 200173860 | Am | 5.454 | 13 | |
| 53 Tau | 200173864 | B9Vsp | 5.482 | 13 | |
| HR 1585 | 200173858 | K1III | 5.49 | 13 | |
| 80 Tau | 200173866 | F0V | 5.552 | 13 | |
| 51 Tau | 200173865 | F0V | 5.631 | 13 | |
| HR 1403 | 200173867 | Am | 5.711 | 13 | |
| 89 Tau | 200173868 | F0V | 5.776 | 13 | |
| HR 1576 | 200173871 | B9V | 5.776 | 13 | |
| 98 Tau | 200173870 | A0V | 5.785 | 13 | |
| 99 Tau | 200173862 | K0III | 5.806 | 13 | |

Table 1 continued on next page

Table 1 (*continued*)

| Name | EPIC | Spectral Type | V (mag) | Campaign | Comments |
|-------------------|-----------|-------------------|------------|----------|----------|
| 105 Tau | 200173869 | B2Ve | 5.92 | 13 | |
| HR 1554 | 200173874 | F2IVn | 5.961 | 13 | |
| HR 1385 | 200173875 | F4V | 5.965 | 13 | C4 |
| HR 1741 | 200173873 | K0III | 6.107 | 13 | |
| HR 1633 | 200173872 | K0 | 6.188 | 13 | |
| HR 1755 | 200173876 | K0III | 6.205 | 13 | |
| ρ Leo | 200182931 | B1Iab | 3.87 | 14 | e |
| 58 Leo | 200182925 | K0.5IIIFe-0.5 | 4.838 | 14 | |
| 48 Leo | 200182926 | G8.5IIIFe-1 | 5.07 | 14 | |
| 53 Leo | 200182928 | A2V | 5.312 | 14 | |
| 65 Leo | 200182927 | K0III | 5.52 | 14 | |
| 35 Sex | 200182929 | K2II-III+K1II-III | 5.79 | 14 | |
| 43 Leo | 200182930 | K3III | 6.08 | 14 | |
| Dschubba | 200194910 | B0.3IV | 2.32 | 15 | |
| Zubenelhakrabi | 200194911 | G8.5III | 3.91 | 15 | |
| ι 1 Lib | 200194912 | B9IVpSi | 4.54 | 15 | b |
| 41 Lib | 200194913 | G8III/IV | 5.359 | 15 | |
| ζ 4 Lib | 200194914 | B3V | 5.499 | 15 | |
| HR 5762 | 200194915 | A2IV | 5.52 | 15 | |
| HR 5806 | 200194916 | K0III | 5.79 | 15 | |
| ζ 3 Lib | 200194917 | K0III | 5.806 | 15 | |
| HR 5810 | 200194918 | K0III | 5.816 | 15 | |
| ι 2 Lib | 200194919 | A2V | 6.066 | 15 | b |
| HR 5620 | 200194920 | K0III | 6.14 | 15 | |
| 28 Lib | 200194921 | G8II/III | 6.17 | 15 | |
| HD 138810 | 200194958 | K1(III)(+G) | 7.02 | 15 | |
| Asellus Australis | 200200356 | K0+IIIb | 3.94 | 16 | |
| Acubens | 200200357 | kA7VmF0/2III/IVSr | 4.249 | 16 | |
| ξ Cnc | 200200358 | G8.5IIIFe-0.5CH-1 | 5.149 | 16 | |
| σ 1 Cnc | 200200360 | A5III | 5.22 | 16 | |
| η Cnc | 200200359 | K3III | 5.325 | 16, 18 | |
| 45 Cnc | 200200728 | A3III:+G7III | 5.65 | 16 | SC |
| σ 2 Cnc | 200200361 | F0IV | 5.677 | 16 | |
| 50 Cnc | 200200363 | A1Vp | 5.885 | 16, 18 | |
| 82 Vir | 200213053 | M1+III | 5.01 | 17 | |
| 76 Vir | 200213054 | G8III | 5.21 | 17 | |
| 68 Vir | 200213055 | K5III | 5.25 | 17 | |
| 80 Vir | 200213056 | K0III | 5.706 | 17 | |

Table 1 continued on next page

Table 1 (*continued*)

| Name | EPIC | Spectral Type | V (mag) | Campaign | Comments |
|--------------|-----------|------------------|------------|----------|----------|
| HR 5106 | 200213057 | A0V | 5.932 | 17 | |
| HR 5059 | 200213058 | A8V | 5.965 | 17 | |
| γ Cnc | 200233186 | A1IV | 4.652 | 18 | C5 |
| ζ Cnc | 200233643 | F8V+G0V | 4.67 | 18 | C5 |
| 60 Cnc | 200233188 | K5III | 5.44 | 18 | C5, C16 |
| 49 Cnc | 200233189 | A1VpHgMnSiEu | 5.66 | 18 | C5 |
| HR 3264 | 200233190 | K1III | 5.798 | 18 | C5 |
| 29 Cnc | 200233192 | A5V | 5.948 | 18 | C5 |
| HR 3222 | 200233193 | G8III | 6.047 | 18 | C5 |
| 21 Cnc | 200233196 | M2III | 6.08 | 18 | C5 |
| 25 Cnc | 200233644 | F5IIIm? | 6.1 | 18 | C5 |
| HR 3558 | 200233195 | K1III | 6.146 | 18 | C5 |
| HR 3541 | 200233194 | C-N4.5 | 6.4 | 18 | C5 |

^aWhite et al. (2017)^bBuysschaert et al. (2018)^cFarr et al. (2018)^dArentoft et al. (2019)^eAerts et al. (2018)¹abCN0.5

Table 2. Global asteroseismic parameters for the 31 red giants for which solar-like oscillations were detected.

| Name | EPIC | ν_{\max} (μHz) | $\Delta\nu$ (μHz) |
|----------------|-----------|------------------------------------|-----------------------------------|
| γ Tau | 200007765 | 62.9 ± 1.4 | 5.6 ± 0.2 |
| $\delta 1$ Tau | 200007766 | 62.6 ± 1.7 | 5.7 ± 0.1 |
| $\nu 2$ Sgr | 200062586 | 7.3 ± 0.1 | 1.3 ± 0.0 |
| o Sgr | 200062589 | 46.3 ± 1.0 | 4.8 ± 0.1 |
| $\xi 2$ Sgr | 200062590 | 11.7 ± 0.6 | 1.9 ± 0.1 |
| τ Sgr | 200062591 | 19.8 ± 0.8 | 2.5 ± 0.1 |
| Albaldah | 200062592 | 47.0 ± 0.4 | 6.0 ± 0.2 |
| ϵ Psc | 200068392 | 33.3 ± 1.2 | 3.6 ± 0.1 |
| HR 8759 | 200164170 | 10.1 ± 0.4 | 1.6 ± 0.1 |
| 81 Aqr | 200164173 | 11.4 ± 0.2 | 1.7 ± 0.1 |
| ϵ Tau | 200173844 | 54.5 ± 1.4 | 5.1 ± 0.1 |
| 75 Tau | 200173852 | 35.0 ± 1.0 | 4.2 ± 0.0 |
| HR 1585 | 200173858 | 9.4 ± 1.0 | 1.5 ± 0.1 |
| 99 Tau | 200173862 | 21.4 ± 1.1 | 2.4 ± 0.1 |
| HR 1755 | 200173876 | 18.8 ± 0.4 | 2.0 ± 0.0 |
| 58 Leo | 200182925 | 17.0 ± 0.5 | 2.0 ± 0.2 |
| 48 Leo | 200182926 | 53.3 ± 0.8 | 5.4 ± 0.0 |
| 65 Leo | 200182927 | 61.6 ± 1.4 | 6.4 ± 0.0 |
| 35 Sex | 200182929 | 11.5 ± 0.1 | 1.5 ± 0.1 |
| 43 Leo | 200182930 | 71.6 ± 2.8 | 7.2 ± 0.1 |
| Zubenelhakrabi | 200194911 | 34.9 ± 1.0 | 3.6 ± 0.1 |
| 41 Lib | 200194913 | 54.3 ± 1.8 | 5.2 ± 0.0 |
| HR 5806 | 200194916 | 53.2 ± 0.8 | 4.9 ± 0.1 |
| $\zeta 3$ Lib | 200194917 | 44.2 ± 1.0 | 3.6 ± 0.3 |
| HR 5810 | 200194918 | 45.0 ± 0.5 | 4.5 ± 0.0 |
| HR 5620 | 200194920 | 96.8 ± 0.7 | 9.3 ± 0.0 |
| 28 Lib | 200194921 | 41.0 ± 0.9 | 4.1 ± 0.2 |
| η Cnc | 200200359 | 22.9 ± 0.9 | 2.7 ± 0.0 |
| 76 Vir | 200213054 | 40.0 ± 2.6 | 3.8 ± 0.1 |
| 80 Vir | 200213056 | 37.0 ± 1.8 | 4.4 ± 0.1 |
| HR 3264 | 200233190 | 22.9 ± 0.2 | 3.0 ± 0.2 |